Fully-implicit algebro-differential parametrization of circuits

Müller Remy, Thomas Hélie

FULLY-IMPLICIT ALGEBRO-DIFFERENTIAL PARAMETRIZATION OF CIRCUITS

Rémy Müller and Thomas Hélie

IRCAM-STMS (UMR 9912)
Sorbonne University
Paris, France
remy.muller@ircam.fr

ABSTRACT

This paper is concerned with the conception of methods tailored for the numerical simulation of power-balanced systems that are well-posed but implicitly described. The motivation is threefold: some electronic components (such as the ideal diode) can only be implicitly described, arbitrary connection of components can lead to implicit topological constraints, finally stable discretization schemes also lead to implicit algebraic equations.

In this paper we start from the representation of circuits using a power-balanced Kirchhoff-Dirac structure, electronic components are described by a local state that is observed through a pair of power-conjugated algebro-differential operators (V, I) to yield the branch voltages and currents, the arc length is used to parametrize switching and non-Lipschitz components, and a power balanced functional time-discretization is proposed. Finally, the method is illustrated on two simple but non-trivial examples.

1. INTRODUCTION

Network analysis of circuits and expression of Kirchhoff laws, naturally leads to implicit differential algebraic equations (DAE). Indeed in the most general form, the branch equations are not described by functions but by *relations* (in the voltage-current plane for algebraic components, voltage-charge for capacitor, current-flux for inductors ...). One of the most general approach is the Sparse Tableau analysis [1] which involves both the nodes and branch variables.

In the study of power-balanced systems, and more generally in the field of geometrical numerical integration, one is not only concerned with the quantitative accuracy of numerical simulations, but also with the qualitative preservation of structural invariants during discretization [2]. It has been shown that the symplectic structure of Hamiltonian systems, responsible for energy preservation, can be generalized to open systems with algebraic constraints by the notion of a Dirac structure [3] [4]. It can even be extended to infinite-dimensional systems such as partial differential equations using a Stokes-Dirac [5] structure. It has been shown in [6] (see also [7] [8]) that Kirchhoff laws generates a Kirchhoff-Dirac structure. Recent work [9] also study the properties and numerical discretization of Port-Hamiltonian DAE systems in descriptor form.

Usually, when possible, DAE are reduced to ordinary differential equations (ODE) or semi-explicit index-1 DAE [10] [8] for which a rich literature of results from system theory and numerical analysis is available to study stability, conservation laws, attraction points, existence and uniqueness of solutions ...

In these reduction processes, a choice has to be made regarding the variables the system is solved for. Choosing the node voltages leads to the Nodal Analysis (NA) method. But it is not sufficient to represent all systems, adding some branch currents leads to the popular Modified Nodal Analysis (MNA) [11]. The importance of state variable choices for computable numerical simulations can be found in [12]. Similar issues are addressed for wave digital filters in [13]. A procedure to guide these choices is the Sequential Causality Assignment Procedure (SCAP) in the bond-graph literature [14]. In the case of switching-circuits, such as those containing ideal diodes or discontinuous laws (see [15]) an approach is to solve for different variables according to the switching state of the system, but the number of such states becomes exponential in the number of switching components.

Since after time discretization, one is left with an algebraic system of (nonlinear) equations which has to be solved by an iterative scheme anyway, the goal of this article, is to propose a structure-preserving power-balanced numerical method capable of dealing with the implicit nature of the network equations.

Section 2 recalls how any electronic circuit can be represented by a Kirchhoff-Dirac structure, uniquely determined by the circuit's incidence matrix. Section 3 describes how to parametrize the (possibly implicit) relation imposed by any circuit component. Power-conjugated voltages and currents (v, i) are obtained by the application of a pair of nonlinear algebro-differential operators (V, I) to a parameter $\boldsymbol{x}$ which stands for the component's local state. In Section 4 arc-length and pseudo arc-length parameterizations[1] are proposed to overcome computational causality problems that arise in switching components and reduce numerical stiffness caused by high Lipschitz constants. In Section 5 a power-balanced and structure preserving time-discretization is presented using a functional framework. This leads to a nonlinear system of algebraic equations which is solved using Newton iteration. Finally two tests circuits are studied in Section 6, a stiff switching diode clipper and a conservative (nonlinear) LCLC circuit with an implicit topological constraint.

2. KIRCHHOFF-DIRAC STRUCTURES FOR CIRCUIT GRAPHS

From a circuit theory perspective, a *Dirac structure* is simply a multi-port that doesn't generate or dissipate power i.e.

$$P = \langle \mathbf{i} \,|\, \mathbf{v} \rangle = 0.$$

Considering components and their interconnections separately, because of Kirchhoff laws, the multi-port connecting all components

[1] Curvilinear coordinates for multi-ports are possible but not addressed.

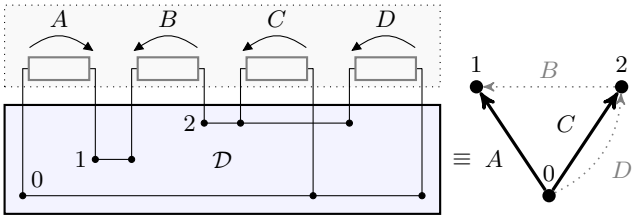

Figure 1: *Dirac structure example with edges* $\mathcal{E} = \{A, B, C, D\}$*, nodes* $\mathcal{N} = \{0, 1, 2\}$ *and chosen spanning tree* $T = \{A, C\}$.

(the PCB) is necessarily a Dirac structure. To formalize it for circuits, we borrow and slightly adapt the notations from [6] [5] [9].

2.1. Circuit Graphs

A directed circuit graph $\mathcal{G}(\mathcal{N}, \mathcal{E})$ is defined by a set of n nodes $\mathcal{N} = \{\eta_1, \dots, \eta_n\}$ and a set $\mathcal{E} = \{\epsilon_1, \dots, \epsilon_m\}$ of m directed edges (links, branches) with no self-loops. Edges are ordered pairs of nodes $\epsilon_i = (\eta_{i,0}, \eta_{i,1})$. Over each node ($k = 0$) and edge ($k = 1$)[2], *using the receiver convention for both*, we define conjugated current and voltages

$$(\mathbf{i}_k, \mathbf{v}_k) \in \mathcal{I}_k \times \mathcal{V}_k =: \mathcal{B}_k, \quad k \in \{0, 1\} \tag{1}$$

where $\mathcal{V}_0 \sim \mathbb{R}^n$, $\mathcal{V}_1 \sim \mathbb{R}^m$ are the spaces of voltages over the nodes $\mathcal{N}$ (resp. the edges $\mathcal{E}$) and $\mathcal{I}_0 = \mathcal{V}_0^*$, $\mathcal{I}_1 = \mathcal{V}_1^*$ the dual spaces of functionals $\mathcal{V}_0 \to \mathbb{R}$, $\mathcal{V}_1 \to \mathbb{R}$. The spaces $\mathcal{B}_0$ and $\mathcal{B}_1$ are respectively the spaces of *bonds* corresponding to the nodes and edges such that power is given by the duality pairings

$$\langle \mathbf{i}_k \,|\, \mathbf{v}_k \rangle_{\mathcal{B}_k} := \mathbf{i}_k^\mathsf{T} \mathbf{v}_k, \qquad k \in \{0, 1\}. \tag{2}$$

Note that since the spaces are finite-dimensional, one can identify each space with its dual $\mathcal{V}_0 \sim \mathcal{I}_0 = \mathbb{R}^n$, $\mathcal{V}_1 \sim \mathcal{I}_0 = \mathbb{R}^m$.

Furthermore, the directed graph is uniquely specified by its (reduced) co-incidence matrix $\mathbf{D}$ given by

$$\mathbf{D} = [d_{ij}]_{m \times n}, \quad d_{i,j} = \begin{cases} 1 & \epsilon_{i,1} = \eta_j \\ -1 & \epsilon_{i,0} = \eta_j \\ 0 & \text{otherwise} \end{cases}. \tag{3}$$

Kirchhoff Current (KCL) and Voltage laws (KVL) [3] can be expressed with an elegant duality (see [16] p.710) using the incidence and coincidence matrices by

$$\mathbf{v}_1 = \mathbf{D}\mathbf{v}_0, \qquad \mathbf{i}_0 = -\mathbf{D}^\mathsf{T}\mathbf{i}_1 = 0. \tag{4}$$

i.e. we have the following diagram.

$$\begin{array}{ccc} \mathbf{v}_0 \in \mathcal{V}_0 & \xrightarrow{\mathbf{D}} & \mathbf{v}_1 \in \mathcal{V}_1 \\ \Big\updownarrow \langle \cdot \,|\, \cdot \rangle_{\mathcal{B}_0} & & \Big\updownarrow \langle \cdot \,|\, \cdot \rangle_{\mathcal{B}_1} \\ \mathbf{i}_0 \in \mathcal{I}_0 & \xleftarrow[-\mathbf{D}^\mathsf{T}]{} & \mathbf{i}_1 \in \mathcal{I}_1 \end{array} \tag{5}$$

[2] This notation is convenient to make the link with automated circuit to Bond-graph algorithms [14]: **0**-junctions (shared voltage, parallel connection) for nodes and **1**-junctions for branches (shared current, serial connection) see Figures 5 and 6 for examples. It is also a mnemonic to remember that lumped circuit equations arise from the spatial discretization of electro-magnetic 1-forms for branches and 0-forms for nodes.

[3] The minus sign in front of $\mathbf{i}_0$ comes from the consistent use of the receiver convention for both nodes and branches: the sum of edge currents $\mathbf{i}_0$ *entering* each node has to be zero.

2.2. Kirchhoff-Dirac structure

Written in matrix form, one obtains the canonical Kirchhoff-Dirac structure $\mathcal{D}$ (with a structure very similar to the ones obtained for partial differential equations (PDE) [17] [5])

$$\mathcal{D} : \begin{bmatrix} \mathbf{i}_0 \\ \mathbf{v}_1 \end{bmatrix} = \begin{bmatrix} \mathbf{0} & -\mathbf{D}^\mathsf{T} \\ \mathbf{D} & \mathbf{0} \end{bmatrix} \begin{bmatrix} \mathbf{v}_0 \\ \mathbf{i}_1 \end{bmatrix}, \quad \mathbf{i}_0 = 0. \tag{6}$$

i.e. Kirchhoff Current Laws can be interpreted as *zero boundary conditions* on the node currents, and the co-incidence matrix $\mathbf{D}$ as a (lumped) differential operator. Left multiplying by $[\mathbf{v}_0 \;\; \mathbf{i}_1]$, the duality products and skew-symmetry leads to the power balance

$$P = \langle \mathbf{i}_0 \,|\, \mathbf{v}_0 \rangle + \langle \mathbf{i}_1 \,|\, \mathbf{v}_1 \rangle = \begin{bmatrix} \mathbf{v}_0 & \mathbf{i}_1 \end{bmatrix} \begin{bmatrix} \mathbf{0} & -\mathbf{D}^\mathsf{T} \\ \mathbf{D} & \mathbf{0} \end{bmatrix} \begin{bmatrix} \mathbf{v}_0 \\ \mathbf{i}_1 \end{bmatrix} = 0.$$

Furthermore since we have conservation of charge $\mathbf{i}_0 = 0$ on the nodes $\mathcal{N}$, this yields the Tellegen theorem over the edges[4] $\mathcal{E}$

$$\langle \mathbf{i}_1 \,|\, \mathbf{v}_1 \rangle = \sum_{\epsilon \in \mathcal{E}} \langle i_\epsilon \,|\, v_\epsilon \rangle = 0.$$

We also remark that the node voltages $\mathbf{v}_0$ can be interpreted as Lagrange multipliers parametrizing the sub-manifold defined by the linear constraints $\mathbf{i}_0 = 0$.

2.3. (Reduced) Hybrid Dirac structure

Whereas MNA solves the system for node voltages and branch currents, in Hybrid Analysis [16] and skew-gradient DAE [7] [8], the node voltages are eliminated. First a spanning tree T is chosen, this yields a partition of the branch currents and voltages into tree $(\mathbf{v}_T, \mathbf{i}_T)$ and link variables $(\mathbf{v}_L, \mathbf{i}_L)$. Partitioning equations according to the spanning tree, Kirchhoff laws (4) are rewritten as

$$\begin{bmatrix} \mathbf{v}_T \\ \mathbf{v}_L \end{bmatrix} = \begin{bmatrix} \mathbf{D}_T \\ \mathbf{D}_L \end{bmatrix} \mathbf{v}_0, \qquad \begin{bmatrix} \mathbf{D}_T^\mathsf{T} & \mathbf{D}_L^\mathsf{T} \end{bmatrix} \begin{bmatrix} \mathbf{i}_T \\ \mathbf{i}_L \end{bmatrix} = 0. \tag{7}$$

From graph theory, having a spanning tree ensures that the matrix $\mathbf{D}_T \in \mathbb{R}^{n \times n}$ is invertible. So we can eliminate the node voltages $\mathbf{v}_0$ using $\mathbf{v}_0 = \mathbf{D}_T^{-1}\mathbf{v}_T$. This yields a reduced Hybrid Dirac structure specified by its link-cutset matrix $\mathbf{C} = (\mathbf{D}_L\mathbf{D}_T^{-1})^\mathsf{T}$

$$\mathcal{D} : \begin{bmatrix} \mathbf{i}_T \\ \mathbf{v}_L \end{bmatrix} = \begin{bmatrix} \mathbf{0} & -\mathbf{C} \\ \mathbf{C}^\mathsf{T} & \mathbf{0} \end{bmatrix} \begin{bmatrix} \mathbf{v}_T \\ \mathbf{i}_L \end{bmatrix}. \tag{8}$$

Traditionally, the spanning tree is chosen to be a proper tree (i.e. containing all current-driven branches: Voltages Sources, Capacitors, …) such that $\mathbf{v}_T$ is current-driven by $\mathbf{i}_T$ (i.e. computable from $\mathbf{i}_T$). However topological constraints such as in example 6.2 may prevent a proper tree to be found. Since the proposed method is fully-implicit by nature, it does not have such a requirement. Either the Kirchhoff-Dirac structure or *any* reduced Hybrid Dirac structure can be used for simulation.

For a formal definition of Dirac structures in the broader context of multi-physical networks, pleaser refer to [6] and references therein. A generic example of a Dirac structure and its graph, emphasizing the node-edge incidence structure, is shown on Figure 1. Detailed case-study are shown on Figures 5 and 6 and studied in Section 6.

[4] Indeed (see [16] p. 30) any two of KCL, KVL and Tellegen theorem implies the third one.

3. ALGEBRO-DIFFERENTIAL PARAMETRIZATION OF COMPONENT LAWS

From now on, for functional discretization purpose, we adopt a Hilbert space viewpoint, and lift Dirac structures over time steps. Consider a time interval $\Omega \subset \mathbb{R}$, the branch voltage and current spaces are lifted to the dual Hilbert spaces $\mathcal{I}_1 \sim \mathcal{V}_1 \subseteq L^2(\Omega)^m$ (L^2 being a pivot space) equipped with the inner (duality) product

$$\langle \mathbf{u} \,|\, \mathbf{v} \rangle := \frac{1}{|\Omega|} \int_\Omega \mathbf{u}(t)^\mathsf{T} \mathbf{v}(t) \,\mathrm{d}t. \tag{9}$$

We assume that branch equations can be parametrized locally by a state $\boldsymbol{x} \in \mathcal{X}_1 \subseteq L^2(\Omega)^m$, *nonlinear differential-algebraic operators* $\boldsymbol{I}_1 : \mathcal{X}_1 \to \mathcal{I}_1, \boldsymbol{V}_1 : \mathcal{X}_1 \to \mathcal{V}_1$ and a law

$$\begin{array}{rccl} F & : & \mathcal{X}_1 & \longrightarrow & \mathcal{B}_1 := \mathcal{I}_1 \times \mathcal{V}_1 \\ & & \boldsymbol{x} & \longmapsto & (\boldsymbol{I}_1(\boldsymbol{x}), \boldsymbol{V}_1(\boldsymbol{x})) \end{array}. \tag{10}$$

Likewise the KCL node boundary conditions (4) can be parametrized by the vector of node voltages $\boldsymbol{\lambda} \in \mathcal{X}_0 \subseteq L^2(\Omega)^n$ and the linear constraint

$$\begin{array}{rccl} B & : & \mathcal{X}_0 & \longrightarrow & \mathcal{B}_0 := \mathcal{I}_0 \times \mathcal{V}_0 \\ & & \boldsymbol{\lambda} & \longmapsto & (\boldsymbol{I}_0, \boldsymbol{V}_0)(\boldsymbol{\lambda}) = (0, \boldsymbol{\lambda}) \end{array}. \tag{11}$$

Composing (6) with (10) (11) we obtain the fully implicit algebro-differential formulation of a Port-Hamiltonian system (PHS)

$$\Sigma = \left\{ \begin{array}{l} (\boldsymbol{I}_0, \boldsymbol{V}_0, \boldsymbol{I}_1, \boldsymbol{V}_1)(\boldsymbol{x}, \boldsymbol{\lambda}) \in \mathcal{B}_1 \times \mathcal{B}_0; \\ N(\boldsymbol{x}) = 0, \quad \forall (\boldsymbol{x}, \boldsymbol{\lambda}) \in \mathcal{X}_1 \times \mathcal{X}_0 \end{array} \right\} \tag{12}$$

defined by the operator $N : \mathcal{X}_0 \times \mathcal{X}_1 \to L^2(\Omega)^{m+n}$

$$N(\boldsymbol{x}, \boldsymbol{\lambda}) = \begin{bmatrix} \mathbf{0} \\ \boldsymbol{V}_1(\boldsymbol{x}) \end{bmatrix} - \begin{bmatrix} \mathbf{0} & -\mathbf{D}^\mathsf{T} \\ \mathbf{D} & \mathbf{0} \end{bmatrix} \begin{bmatrix} \boldsymbol{\lambda} \\ \boldsymbol{I}_1(\boldsymbol{x}) \end{bmatrix}. \tag{13}$$

For the reduced Hybrid Dirac structure one gets

$$\Sigma = \left\{ (\boldsymbol{I}_T, \boldsymbol{V}_T, \boldsymbol{I}_C, \boldsymbol{V}_C)(\boldsymbol{x}) \in \mathcal{B}_1 \,|\, N(\boldsymbol{x}) = 0, \, \forall \boldsymbol{x} \in \mathcal{X}_1 \right\} \tag{14}$$

with the algebro-differential operator $N : \mathcal{X}_1 \to L^2(\Omega)^m$

$$N(\boldsymbol{x}) = \begin{bmatrix} \boldsymbol{I}_T(\boldsymbol{x}) \\ \boldsymbol{V}_C(\boldsymbol{x}) \end{bmatrix} - \begin{bmatrix} \mathbf{0} & -\mathbf{C} \\ \mathbf{C}^\mathsf{T} & \mathbf{0} \end{bmatrix} \begin{bmatrix} \boldsymbol{V}_T(\boldsymbol{x}) \\ \boldsymbol{I}_C(\boldsymbol{x}) \end{bmatrix}. \tag{15}$$

We note that for differential components, the state space is given by the Sobolev space $\mathcal{X} \subseteq H^1(\Omega) \subset L^2(\Omega)$ defined by

$$\mathcal{X} = \left\{ x \in L^2(\Omega) \;\middle|\; \dot{x} \in L^2(\Omega); \; x(t) = x_0 + \int_0^t \dot{x}(s) \,\mathrm{d}s \right\}, \tag{16}$$

whereas for algebraic components, no additional smoothness is implied so $\mathcal{X} \sim L^2(\Omega)$.

The differential-algebraic operators corresponding to common electronic components are summarized in Table 1 and the case of implicitly parametrized algebraic components is now further detailed in Section 4.

4. (PSEUDO) ARC-LENGTH PARAMETRIZATION

We study here implicit arc-length and pseudo arc-length parameterizations of algebraic components whose laws cannot be represented as functions of either current or voltage (or such that unbounded Lipschitz constants may cause numerical problems during simulations). As an example we consider the cases of the ideal diode, a nonlinear resistor and the Shockley diode.

4.1. The ideal diode

An ideal diode law is determined by the set (see [15])

$$\mathcal{R}_D = \left\{ (v, i) \in \mathbb{R}^2 \;\middle|\; \begin{cases} v = 0 & i \in \mathbb{R}^+, \\ i = 0 & v \in \mathbb{R}^-. \end{cases} \right\} \tag{17}$$

It has the numerical disadvantage of being alternatively voltage and current controlled. In the hybrid formulation, computational causality assignment [14] would imply that a different Dirac structure such as (8) should be used according to the current state of the circuit. Furthermore, when the number of switching components grows, the number of switch configurations of the circuit grows exponentially. A solution around this problem is to consider the parametrization $R_D : \lambda \mapsto (V_D(\lambda), I_D(\lambda))$ with arc-length

$$\lambda(v, i) = \begin{cases} i/I_0 & v = 0, \; i \in \mathbb{R}^+ \\ v/V_0 & i = 0, \; v \in \mathbb{R}^- \end{cases}, \tag{18}$$

for arbitrarily chosen positive reference current and voltages I_0, V_0. Inverting the relation, one obtains the algebraic operators

$$V_D(\lambda) = V_0 \min(\lambda, 0), \qquad I_D(\lambda) = I_0 \max(\lambda, 0). \tag{19}$$

with $V_D'(\lambda) = V_0 \cdot \mathbf{1}_{\mathbb{R}^-}(\lambda)$, and $I_D'(\lambda) = I_0 \cdot \mathbf{1}_{\mathbb{R}^+}(\lambda)$, where $\mathbf{1}_A(\lambda)$ denotes the indicator function of a set A.

Differential	x	$V(x)$	$I(x)$	$H(x)$
Capacitor	q	q/C	$\dot{q}$	$q^2/2\mathsf{C}$
Inductor	ϕ	$\dot{\phi}$	ϕ/L	$\phi^2/2\mathsf{L}$
Nonlinear Capacitor	q	$\nabla H(q)$	$\dot{q}$	$H(q)$
Nonlinear Inductor	ϕ	$\dot{\phi}$	$\nabla H(\phi)$	$H(\phi)$

Algebraic	x	$V(x)$	$I(x)$	$P(x)$
Resistor	i	$\mathsf{R}i$	i	$\mathsf{R}i^2$
Conductor	v	v	$\mathsf{G}v$	$\mathsf{G}v^2$
Nonlinear Resistor	i	$z(i)$	i	$i \cdot z(i)$
Nonlinear Conductor	v	v	$z(v)$	$v \cdot z(v)$
Voltage source	i	V	i	$\mathsf{V} \cdot i$
Current source	v	v	I	$\mathsf{I} \cdot v$

Table 1: *Differential and Algebraic components. H (energy), P (power), q (charge), ϕ (flux), z (non linear function).*

4.2. A Hard Clipping resistor

We now consider the case of a hard clipping resistor (it will be used in example 6.1) whose (v,i) graph is described by the set

$$\mathcal{R}_D = \left\{ (v,i) \in \mathbb{R}^2;\ \begin{cases} i \in \mathbb{R}^- \setminus \{0\} & v \in \{-1\} \\ i \in \{0\} & v \in (-1,1) \\ i \in \mathbb{R}^+ \setminus \{0\} & v \in \{1\} \end{cases} \right\}. \quad (20)$$

We parametrize it continuously using (see Figure 4 page 8)

$$\mathcal{R}_D = \left\{ (v,i) \in \mathbb{R}^2; \quad (v,i) = (V(\lambda), I(\lambda)), \quad \forall \lambda \in \mathbb{R} \right\} \quad (21)$$

with the voltage and current operators

$$V(\lambda) = V_0 \operatorname{clip}_{[-1,1]}(\lambda), \quad (22)$$

$$I(\lambda) = I_0 \left(\min(0, \lambda + 1) + \max(0, \lambda - 1) \right). \quad (23)$$

For arbitarily chosen positive reference voltage and currents V_0, I_0.

4.3. The Shockley diode

We finally consider the Shockley diode model [5].

$$I(v) = I_S \left(\exp\left(\frac{v}{V_T} \right) - 1 \right), \quad (24)$$

where I_S is the saturation current, $V_T = k_b T / q_e$ the thermal voltage, with temperature T, Boltzmann constant k_b and electron charge q_e. It is $\mathcal{C}^\infty$-continuous, but not globally Lipschitz.

For a chosen reference resistance R_0, the true arc-length of the graph $(v, R_0 I(v))$ is determined by $\mathrm{d}\lambda^2 = (1 + (R_0 I'(v))^2)\,\mathrm{d}v^2$ but it is not practical to manipulate. Instead, introducing the diode cutoff point (V_0, I_0) as the point of unit slope

$$R_0 I'(V_0) = 1, \qquad I_0 = I(V_0), \quad (25)$$

where $V_0 = V_T \ln\left(\frac{V_T}{R_0 I_S}\right)$, $I_0 = V_T / R_0 - I_S$. Remarking that for $v \ll V_0$, $\mathrm{d}\lambda \approx \mathrm{d}v$ and for $v \gg V_0$, $\mathrm{d}\lambda \approx R_0 I'(v)\,\mathrm{d}v$, one can introduce the $\mathcal{C}^0$ pseudo arc-length differential

$$\mathrm{d}\tilde{\lambda}(v) = \begin{cases} \mathrm{d}v & v < V_0 \\ R_0 I'(v)\,\mathrm{d}v & v \geq V_0 \end{cases}. \quad (26)$$

Integrating $\tilde{\lambda}(v) := \int_0^v \mathrm{d}\tilde{\lambda}$ one obtains the $\mathcal{C}^1$ pseudo-arclength

$$\tilde{\lambda}(v) = \begin{cases} v & v < V_0 \\ V_0 + R_0 (I(v) - I_0), & v \geq V_0. \end{cases} \quad (27)$$

Inverting the relation leads to the algebraic operators

$$V_D(\lambda) = \begin{cases} \lambda & \lambda < V_0, \\ V_T \ln\left(1 + \dfrac{I_0 + (\lambda - V_0)/R_0}{I_S}\right) & \lambda \geq V_0, \end{cases} \quad (28)$$

$$I_D(\lambda) = \begin{cases} I(\lambda) & \lambda < V_0, \\ I_0 + \dfrac{\lambda - V_0}{R_0} & \lambda \geq V_0 \end{cases}. \quad (29)$$

[5] Anti-parallel Shockley diodes will be simulated in example 6.1

such that by construction, Lipschitz constants are unitary (this property is key to deal with convergence and numerical stiffness)

$$L_V = \sup_\lambda \left| V_D' \right| = 1, \qquad L_I = \sup_\lambda \left| R_0 I_D' \right| = 1. \quad (30)$$

5. FUNCTIONAL DISCRETIZATION AND NUMERICAL SOLVER

We now use the functional framework presented in Section 3 to discretize the system with a finite number of parameters per time step, (see the reference [18] for the representation of non band-limited signals having a *finite rate of innovation*).

Our time discretisation scheme can be interpreted as an extension of (spectral) time-finite elements methods [19] to DAE. It is based on the following theorem which proves that a weak PHS is preserved over the chosen approximation subspace.

Theorem 5.1 (Weak PHS)**.** *Let Ω be a time step, $\boldsymbol{x} \in \mathcal{X} \subseteq L^2(\Omega)^m$ a functional state, two operators $\boldsymbol{b} : \mathcal{X} \to L^2(\Omega)^m$, $\boldsymbol{a} : \mathcal{X} \to L^2(\Omega)^m$ and a skew-symmetric matrix $\mathbf{J}$ defining the PHS operator*

$$N(\boldsymbol{x}) = \boldsymbol{b}(\boldsymbol{x}) - \mathbf{J}\boldsymbol{a}(\boldsymbol{x}) = 0, \quad \mathbf{J} = -\mathbf{J}^*. \quad (31)$$

Let $\boldsymbol{P} : L^2(\Omega) \to R(\boldsymbol{P}) \subseteq L^2(\Omega)^m$ be a projector ($\boldsymbol{P}^2 = \boldsymbol{P}$) satisfying the skew-adjoint commutation $\boldsymbol{P}\mathbf{J} = \mathbf{J}\boldsymbol{P}^*$, for the L^2 inner product (9)*, then the projected operator*

$$\boldsymbol{P} \circ N(\boldsymbol{x}) = 0 \quad (32)$$

defines a weak PHS which preserves the power balance.

$$\left\langle \boldsymbol{a}(\boldsymbol{x}) \,\middle|\, \boldsymbol{P} \,\middle|\, \boldsymbol{b}(\boldsymbol{x}) \right\rangle = 0. \quad (33)$$

Proof. Using (32), taking the inner product with $\boldsymbol{a}(\boldsymbol{x})$, and using the fact that 1) $\boldsymbol{P}^2 = \boldsymbol{P}$ (idempotence), 2) we have the commutation $\boldsymbol{P}\mathbf{J} = \mathbf{J}\boldsymbol{P}^*$ and 3) $\boldsymbol{P}\mathbf{J}\boldsymbol{P}^*$ is skew-adjoint, we obtain

$$\begin{aligned} & \left\langle \boldsymbol{a}(\boldsymbol{x}) \,\middle|\, \boldsymbol{P} \,\middle|\, N(\boldsymbol{x}) \right\rangle = 0 \\ \iff & \left\langle \boldsymbol{a}(\boldsymbol{x}) \,\middle|\, \boldsymbol{P} \,\middle|\, \boldsymbol{b}(\boldsymbol{x}) \right\rangle = \left\langle \boldsymbol{a}(\boldsymbol{x}) \,\middle|\, \boldsymbol{P}\mathbf{J} \,\middle|\, \boldsymbol{a}(\boldsymbol{x}) \right\rangle \\ & \qquad \overset{1}{=} \left\langle \boldsymbol{a}(\boldsymbol{x}) \,\middle|\, \boldsymbol{P}^2\mathbf{J} \,\middle|\, \boldsymbol{a}(\boldsymbol{x}) \right\rangle \\ & \qquad \overset{2}{=} \left\langle \boldsymbol{a}(\boldsymbol{x}) \,\middle|\, \boldsymbol{P}\mathbf{J}\boldsymbol{P}^* \,\middle|\, \boldsymbol{a}(\boldsymbol{x}) \right\rangle \overset{3}{=} 0. \end{aligned}$$

□

Remark (Energy conservation)**.** As an immediate consequence, for a conservative Hamiltonian system given by the operator

$$N(\boldsymbol{x}) = \frac{\mathrm{d}\boldsymbol{x}}{\mathrm{d}t} - \mathbf{J}\nabla H(\boldsymbol{x}) = 0, \quad \mathbf{J} = -\mathbf{J}^T. \quad (34)$$

discretized such that $\dot{\boldsymbol{x}} = \boldsymbol{P}\mathbf{J}\nabla H(\boldsymbol{x})$, then the Hamiltonian energy H is preserved over a time-step $\Omega = (t_0, t_1)$,

$$H(\boldsymbol{x}(t_1)) - H(\boldsymbol{x}(t_0)) = 0. \quad (35)$$

Indeed, let $\boldsymbol{b} = \frac{\mathrm{d}}{\mathrm{d}t}$ and $\boldsymbol{a} = \nabla H$, from the gradient theorem and using the same arguments as the previous proof, it follows that

$$\begin{aligned} H(\boldsymbol{x}(t_1)) - H(\boldsymbol{x}(t_0)) &= \left\langle \nabla H(\boldsymbol{x}) \,\middle|\, \dot{\boldsymbol{x}} \right\rangle \\ &= \left\langle \nabla H(\boldsymbol{x}) \,\middle|\, \boldsymbol{P}\mathbf{J}\boldsymbol{P}^* \,\middle|\, \nabla H(\boldsymbol{x}) \right\rangle = 0. \end{aligned}$$

5.1. Piecewise constant and affine polynomial spaces

In this article we will restrict ourselves to constant and affine polynomial spaces $\mathbb{P}^0, \mathbb{P}^1$ for which we have *exact closed-form* expression of the projected operators. (Higher-order polynomial spaces require the use of approximate quadratures rules [2] [9]). Results are exposed without proof except when the proof is not available elsewhere (see [8]).

Consider a unit time step $\Omega = (0, 1)$, for the normalized time variable $\tau \in (0, 1)$ and two orthogonal polynomials

$$\ell_0(\tau) = 1, \qquad \ell_1(\tau) = \tau - \frac{1}{2}.$$

The operator $P_K : L^2(\Omega) \to \mathbb{P}^K(\Omega) \subset L^2(\Omega)$, $K \in \{0, 1\}$ defined by

$$(P_K\, u)(\tau) = \sum_{i=0}^{K} \ell_i(\tau) \frac{\langle \ell_i \,|\, u \rangle}{\langle \ell_i \,|\, \ell_i \rangle} \tag{36}$$

is an orthogonal projector. i.e. P_K is self-adjoint ($P_K = P_K^*$) and idempotent ($P_K^2 = P_K$). For notational simplicity, we define the following notation. Let $A : L^2(\Omega) \to L^2(\Omega)$ be an operator, the *projected operator* $\bar{A}_K : L^2(\Omega) \to \mathbb{P}^K(\Omega)$ is defined by

$$\bar{A}_K := P_K \circ A, \quad \bar{A} := \bar{A}_0. \tag{37}$$

By extension, for a vectorized projector $\boldsymbol{P} := P_K \otimes \mathbf{I}_n$, it yields the projected PHS operator

$$\overline{N}(\boldsymbol{x}) := \boldsymbol{P} \circ N(\boldsymbol{x}) \tag{38}$$

Because of the tensor product construction, we also have the commutation $\boldsymbol{P}\mathbf{J} = \mathbf{J}\boldsymbol{P} = \mathbf{J}\boldsymbol{P}^*$ such that $\boldsymbol{P}$ satisfies Theorem 5.1.

For numerical computations, it is necessary to compute the polynomial coefficients of the image of a trajectory through a nonlinear function. This is possible thanks to the following property

Property 5.1 (Projected function)**.** Let $f : \mathbb{R} \to \mathbb{R}$ be a semi-continuous function with known antiderivative F and a function

$$x(\tau) = \ell_0(\tau)\bar{x} + \ell_1(\tau)\delta x \;\in\; \mathbb{P}^1(\Omega), \tag{39}$$

parametrized by its mean and variation $\Theta = (\bar{x}, \delta x) \in \mathbb{R}^2$

Then the projected function $P_1 \circ f \circ x$ has the projection coefficients $\overline{\mathbf{f}} : \mathbb{R}^2 \to \mathbb{R}^2$ defined by

$$\overline{\mathbf{f}}_i := \langle \ell_i \,|\, f \circ x \rangle \,/ \|\ell_i\|^2 . \tag{40}$$

They are given in closed form by

$$\overline{\mathbf{f}}_0(\Theta) = \begin{cases} \dfrac{F(\bar{x} + \frac{\delta x}{2}) - F(\bar{x} - \frac{\delta x}{2})}{\delta x} & \delta x \neq 0 \\ \dfrac{f(\bar{x}^+) + f(\bar{x}^-)}{2} & \delta x = 0 \end{cases} \tag{41}$$

$$\overline{\mathbf{f}}_1(\Theta) = \begin{cases} \dfrac{12}{\delta x}\left(\dfrac{F(x_1) + F(x_0)}{2} - \overline{\mathbf{F}}_0(\Theta)\right) & \delta x \neq 0 \\ 0 & \delta x = 0 \end{cases} \tag{42}$$

where $x_1 = \bar{x} + \delta x/2$, $x_0 = \bar{x} - \delta x/2$.

Proof. See Appendix A. □

Note that for a scalar (or separable) potential F, using $f = \nabla F$, and $\bar{x} = (x_0 + x_1)/2$, $\delta x = x_1 - x_0$ in property 5.1 yields the *Average Discrete Gradient* from [8] (this is also an instance of anti-derivative anti-aliasing)

$$\overline{\nabla} F(x_0, x_1) := \overline{\mathbf{f}}_0(\Theta). \tag{43}$$

Additional results for linear gradients are given in appendix B.

5.2. Newton iteration

For each time step Ω, let Θ denote the unknown parameters of a local state $\boldsymbol{x}_\Theta \in (\mathbb{P}^K(\Omega))^m$ we look for a zero $\overline{\mathbf{N}}(\Theta^\star) = 0$ of

$$\overline{\mathbf{N}}(\Theta) := \left[\langle \ell_i \,|\, N(\boldsymbol{x}_\Theta)\rangle \,/ \|\ell_i\|^2\right]_{i=0\ldots K} \tag{44}$$

using Newton iteration (line search is not used in this paper)

$$\Theta_{\kappa+1} = \Theta_\kappa + \Delta\Theta_\kappa, \quad \Delta\Theta_\kappa = -\overline{\mathbf{N}}'(\Theta_\kappa)^{-1}\overline{\mathbf{N}}(\Theta_\kappa). \tag{45}$$

A detailed convergence analysis for the general case is out of the scope this paper and is left for future work. Please refer to [20] for more details. When $\overline{\mathbf{N}}$ is only semi-smooth which is the case of the ideal and hard clipping diodes, special care should be taken to ensure convergence using semi-smooth Newton methods [21].

It should be noted that in piecewise constant spaces ($k = 0$), algebraic constraints simplifies to $\overline{\mathbf{V}}(\mathbf{s}) = V(s)$, $\overline{\mathbf{I}}(\mathbf{s}) = I(s)$, and one can compute the Jacobian from the derivative V', I'. For affine trajectories ($k = 1$) one should use the results from properties 5.1 and the following property from [8] to compute the coefficients and the Jacobian.

Property 5.2. Given a potential $F \in C^2(\mathbb{R}, \mathbb{R})$, and its discrete gradient $\overline{\nabla} F(x_0, x_1)$ defined in Equation (43), the derivative of the discrete gradient with respect to x_1 is

$$\frac{\partial \overline{\nabla} F}{\partial x_1} = \begin{cases} \dfrac{\nabla F(x_1) - \overline{\nabla} F(x_0, x_1)}{x_1 - x_0} & x_0 \neq x_1 \\ \dfrac{1}{2}\dfrac{\partial^2 F}{\partial x^2}(x_0) & x_0 = x_1 \end{cases}. \tag{46}$$

6. EXAMPLES

6.1. Diode Clipper

We consider the diode clipper circuit shown in Figure 5. This circuit which is dissipatively stiff because of the diode unbounded Lipschitz constant is commonly used to benchmark numerical schemes. In this paper the nonlinear resistor D is considered abstract and will be substituted by anti-parallel Shockley and hard clipping diode models from Section 4.

Over each time step it is parametrized by the vector of Legendre coefficients $\Theta = (\mathbf{i}_S, \mathbf{i}_C, \mathbf{v}_R, \mathbf{x}_D) \in (\mathbb{R}^{K+1})^4$, for $K \in \{0, 1\}$ and the functional state $\boldsymbol{x}_\Theta = [i_S, i_C, v_R, x_D]^T \in (\mathbb{P}^K(\Omega))^4$ such that each element $v \in \mathbb{P}^K(\Omega)$ is of the form $v(t_0 + h\tau) = \sum_{n=0}^{K} \ell_n(\tau)\mathbf{v}[n]$. The projected Dirac structure (where $\mathbf{1}$ is the identity on $\mathbb{R}^{K+1}$) is then given by the operator

$$\overline{\mathbf{N}} = \begin{bmatrix} \mathbf{i}_S \\ \mathbf{i}_C \\ \mathbf{v}_R \\ \overline{\mathbf{V}}_D(\mathbf{x}_D) \end{bmatrix} - \begin{bmatrix} . & . & -\mathbf{1} & \mathbf{0} \\ . & . & \mathbf{1} & -\mathbf{1} \\ \mathbf{1} & -\mathbf{1} & . & . \\ \mathbf{0} & \mathbf{1} & . & . \end{bmatrix} \begin{bmatrix} \overline{\mathbf{V}}_S \\ \overline{\mathbf{V}}_C(\mathbf{i}_C) \\ \overline{\mathbf{I}}_R(\mathbf{v}_R) \\ \overline{\mathbf{I}}_D(\mathbf{x}_D) \end{bmatrix}. \tag{47}$$

Results are shown on Figure 2 for an input $v_S = V \sin(2\pi f_0 t)$ with high input gain $V = 10^4$, fundamental frequency $f_0 = 500$ Hz, $R = 1$ kΩ , $C = 10\mu$F, $I_S = 100$ fA, $R_0 = 0.1\Omega$, sampling frequency $f_s = 96$ kHz. Anti-parallel Shockley diodes with arc length converge on average in 2 iterations and 4 times reduction of the worst-case iteration count (Newton tolerance $\epsilon_r = 10^{-5}$), Hard clipping diodes exhibit convergence in one iteration most of the time (2 when switching) even for $\epsilon_r = 10^{-10}$.

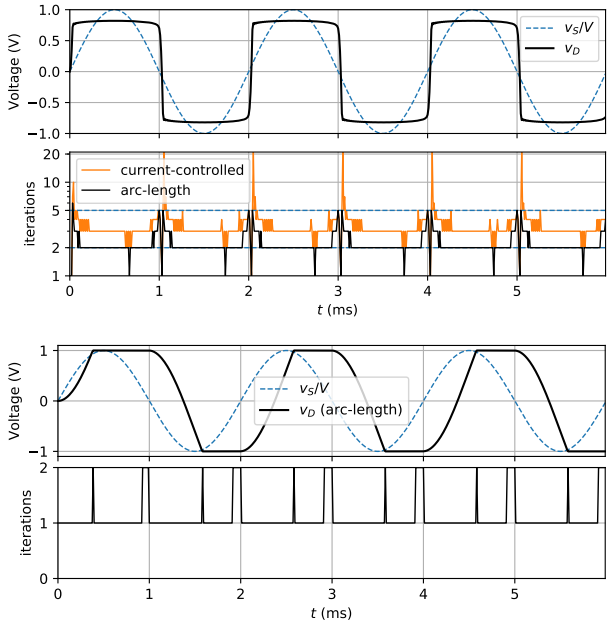

Figure 2: *Diode clipper: anti-parallel Shockley diodes (top) with $V = 10^4$ to emphasize Newton iteration differences, Hard clipping diodes (bottom) $V = 10^2$ to see dynamic and saturation.*

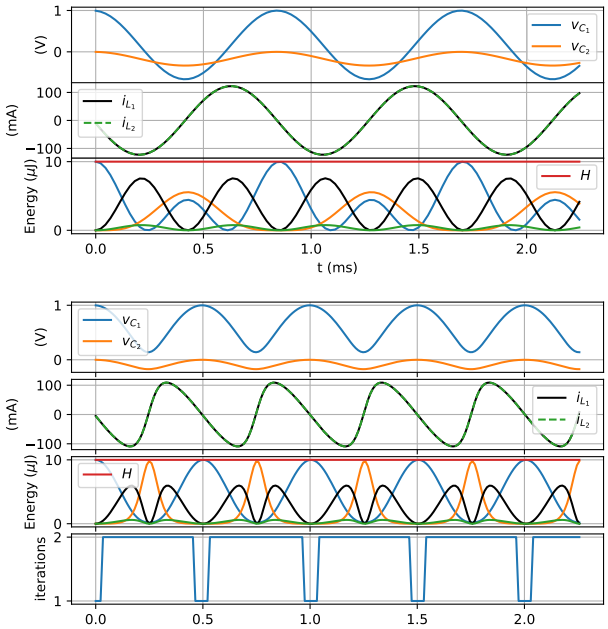

Figure 3: *Conservative LCLC circuit: Linear (top) and Nonlinear (bottom). Notice the periodicity change and conserved energy.*

6.2. LCLC circuit

We study here an LCLC circuit (shown on Figure 6) chosen to demonstrate the proposed method when the circuit is conservative, nonlinear and contains topological constraints (parallel capacitors, serial inductors ...). Here the circuit contains two inductors with the implicit topological constraint $i_{L_1} = i_{L_2}$.

In traditional solvers, such constraints usually needs to be detected and eliminated before proceeding to simulation. A possible approach is the use of equivalent macro components (see [22] [23]). In contrast, the proposed approach doesn't require such a preprocessing step, and keeps the modularity and sparsity of the component-based description. To demonstrate energy conservation, the capacitor C_2 is chosen first with a linear law $V_{C_2}(q) = q/C_2$ and an hardening nonlinearity $V_{C_2}(q) = V_\alpha \sinh(\frac{q}{C_2 V_\alpha})$ with $V_\alpha = 1/30$ (V).

Using the vector of Legendre coefficients as unknown $\Theta = (\mathbf{i}_{C_1}, \mathbf{v}_{L_1}, \mathbf{i}_{C_2}, \mathbf{v}_{L_2})$, we have the projected Dirac structure operator

$$\overline{\mathbf{N}} = \begin{bmatrix} \mathbf{i}_{C1} \\ \overline{\mathbf{I}}_{L1}(\mathbf{v}_{L1}) \\ \mathbf{i}_{C2} \\ \mathbf{v}_{L2} \end{bmatrix} - \begin{bmatrix} . & . & . & \mathbf{1} \\ . & . & . & \mathbf{1} \\ . & . & . & \mathbf{1} \\ \mathbf{-1} & \mathbf{-1} & \mathbf{-1} & . \end{bmatrix} \begin{bmatrix} \overline{\mathbf{V}}_{C1}(\mathbf{i}_{C1}) \\ \mathbf{v}_{L1} \\ \overline{\mathbf{V}}_{C2}(\mathbf{i}_{C2}) \\ \overline{\mathbf{I}}_{L2}(\mathbf{v}_{L2}) \end{bmatrix} \quad (48)$$

Simulation results are shown for the implicit and nonlinear LCLC circuit on Figure 3 for $f_s = 88.2$ kHz, $C_1 = 20\mu$F, $C_2 = 100\mu$F, $L_1 = 1$mH, $L_2 = 100\mu$H, zero initial conditions and $v_{C_1}(0) = 1$V. We observe that both the algebraic constraint $i_{L_1} = i_{L_2}$ and the conservation of total energy H are respected. Convergence is reached in 1 iteration for the linear case and between 1 and 2 iterations for the nonlinear one (relative tolerance $\epsilon_r = 10^{-5}$).

7. CONCLUSIONS

A new power-balanced, fully implicit component oriented method has been presented with a functional time-discretization. Its main strengths (not necessarily unique to this method) are: a) it retains the topological sparsity and modularity of the network based description, b) it is power-balanced and energy-conserving (including nonlinear components), c) it can deal with implicit topological constraints (capacitor loops, inductor cutsets) without the need of manual substitution of equivalent components, d) it can deal with implicit components including switching components, e) it uses finite-dimensional subspace projection as a unifying discretization tool common to ODE, PDE and DAE. f) Newton iteration converges faster using arc-length description of algebraic components with unbounded Lipschitz constants,

Regarding perspectives, a detailed convergence study of the Newton iteration is needed (such as the one in [24]), but has been postponed for future work. Using different and higher order functional approximation spaces is also an obvious perspective provided the projections can be computed exactly and efficiently. In particular, from a generalized sampling theory viewpoint, it would be interesting to perform a comparative analysis of implementation cost and convergence rate (to the true solution) between functional projection and oversampling.

8. REFERENCES

[1] G. Hachtel, R. Brayton, and F. Gustavson, "The sparse tableau approach to network analysis and design," *IEEE Transactions on Circuit Theory*, vol. 18, no. 1, pp. 101–113, 1971.

[2] E. Celledoni and E. H. Høiseth, "Energy-preserving and passivity-consistent numerical discretization of port-

Hamiltonian systems," *arXiv preprint arXiv:1706.08621*, 2017.

[3] I. Y. Dorfman, "Dirac structures of integrable evolution equations," *Physics Letters A*, vol. 125, no. 5, pp. 240–246, 1987.

[4] T. Courant and A. Weinstein, "Beyond Poisson structures," *Action hamiltoniennes de groupes. Troisieme théoreme de Lie*, vol. 27, pp. 39–49, 1988.

[5] P. Kotyczka, B. Maschke, and L. Lefèvre, "Weak form of Stokes–Dirac structures and geometric discretization of port-Hamiltonian systems," *Journal of Computational Physics*, vol. 361, pp. 442–476, 2018.

[6] A. van der Schaft and D. Jeltsema, "Port-Hamiltonian systems theory: An introductory overview," *Foundations and Trends in Systems and Control*, vol. 1, no. 2-3, pp. 173–378, 2014.

[7] A. Falaize and T. Hélie, "Passive guaranteed simulation of analog audio circuits: A port-Hamiltonian approach," *Applied Sciences*, vol. 6, no. 10, 2016.

[8] R. Muller and T. Hélie, "Power-balanced modelling of circuits as skew gradient systems," in *Proc. 21th Conf. Digital Audio Effects*, 2018.

[9] V. Mehrmann and R. Morandin, "Structure-preserving discretization for port-Hamiltonian descriptor systems," *arXiv preprint arXiv:1903.10451*, 2019.

[10] M. Holters and U. Zölzer, "A generalized method for the derivation of non-linear state-space models from circuit schematics," in *2015 23rd European Signal Processing Conference (EUSIPCO)*, pp. 1073–1077, 2015.

[11] C.-W. Ho, A. Ruehli, and P. Brennan, "The modified nodal approach to network analysis," *IEEE Transactions on Circuits and Systems*, vol. 22, no. 6, pp. 504–509, 1975.

[12] T. Serafini and P. Zamboni, "State variable changes to avoid non computational issues," *Available on-line at http://www.simulanalog.org/statevariable.pdf (checked April 15, 2020)*.

[13] K. J. Werner, M. J. Olsen, M. Rest, and J. Parker, "Generalizing root variable choice in wave digital filters with grouped nonlinearities," in *Proc. 20th Int. Conf. Digit. Audio Effects, Edinburgh, UK*, 2017.

[14] P. C. Breedveld, "A systematic method to derive bond graph models," in *Proc. of the 2nd European Simulation Congress*, pp. 38–44, 1986.

[15] V. Acary, O. Bonnefon, and B. Brogliato, *Nonsmooth modeling and simulation for switched circuits*, vol. 69. Springer Science & Business Media, 2010.

[16] L. O. Chua, C. A. Desoer, and E. S. Kuh, *Linear and nonlinear circuits*. 1987.

[17] B. Jacob and H. J. Zwart, *Linear port-Hamiltonian systems on infinite-dimensional spaces*, vol. 223. Springer Science & Business Media, 2012.

[18] P. L. Dragotti, M. Vetterli, and T. Blu, "Sampling moments and reconstructing signals of finite rate of innovation: Shannon meets strang–fix," *IEEE Transactions on Signal Processing*, vol. 55, no. 5, pp. 1741–1757, 2007.

[19] W. Tang and Y. Sun, "Time finite element methods: A unified framework for numerical discretizations of ODEs," *Applied Mathematics and Computation*, vol. 219, no. 4, pp. 2158–2179, 2012.

[20] P. Deuflhard, *Newton methods for nonlinear problems: Affine invariance and adaptive algorithms*, vol. 35. Springer, 2011.

[21] M. Hintermüller, "Semismooth Newton methods and applications," tech. rep., Department of Mathematics, Humboldt-University of Berlin, 2010.

[22] J. Najnudel, T. Hélie, H. Boutin, D. Roze, T. Maniguet, and S. Vaiedelich, "Analog circuits and port-Hamiltonian realizability issues: A resolution method for simulations via equivalent components," in *Audio Engineering Society Convention 145*, 2018.

[23] J. Najnudel, T. Hélie, and D. Roze, "Simulation of the ondes martenot ribbon-controlled oscillator using energy-balanced modeling of nonlinear time-varying electronic components," *Journal of the Audio Engineering Society*, vol. 67, no. 12, pp. 961–971, 2019.

[24] F. Fontana and E. Bozzo, "Newton–raphson solution of nonlinear delay-free loop filter networks," *IEEE/ACM Transactions on Audio, Speech, and Language Processing*, vol. 27, no. 10, pp. 1590–1600, 2019.

A. PROOF OF PROPERTY 5.1

The proof of Equation (41) is available in [8] and is not reproduced here. To prove its extension to semi-continuous functions, using left and right Taylor series expansion one finds

$$\begin{aligned}\lim_{\delta x\to 0}\overline{\mathbf{f}}_0(\mathbf{x}) &= \lim_{\delta x\to 0}\frac{F(\bar{x}+\frac{\delta x}{2})-F(\bar{x}-\frac{\delta x}{2})}{\delta x}\\ &= \lim_{\delta x\to 0}\frac{f(\bar{x}+\frac{\delta x}{2})\frac{\delta x}{2}+f(\bar{x}-\frac{\delta x}{2})\frac{\delta x}{2}+\mathcal{O}(|\delta x|^2)}{\delta x}\\ &= \frac{f(\bar{x}^+)+f(\bar{x}^-)}{2}.\end{aligned}$$

For the second coefficient, one finds $\|\ell_1\|^2 = 1/12$ and using integration by parts, one gets the recursive relation

$$\begin{aligned}\overline{\mathbf{f}}_1(\mathbf{x}) &= \int_0^1 \ell_1(\tau)f(x(\tau))\,\mathrm{d}\tau = \frac{1}{\delta x}\int_0^1 \ell_1(\tau)\,(F\circ x)'\,(\tau)\,\mathrm{d}\tau\\ &= \frac{1}{\delta x}\left(\left[\ell_1(\tau)(F\circ x)(\tau)\right]_0^1 - \int_0^1 (F\circ x)\,(\tau)\,\mathrm{d}\tau\right)\\ &= \frac{1}{\delta x}\left(\frac{F(x_1)+F(x_0)}{2} - \overline{\mathbf{F}}_0(\mathbf{x})\right).\end{aligned}$$

Finally, when $\delta x = 0$, one finds

$$\overline{\mathbf{f}}_1(\mathbf{x}) = \int_0^1 \ell_1(\tau)f(\bar{x})\,\mathrm{d}\tau = f(\bar{x})\int_0^1 \ell_1(\tau)\,\mathrm{d}\tau = 0.$$

B. LINEAR DIFFERENTIAL COMPONENTS

When $\nabla H(\boldsymbol{x}) = \mathbf{W}\boldsymbol{x}$ with state $\dot{\boldsymbol{x}}(\tau) \in \mathbb{P}^1$ and coefficients $\dot{\mathbf{x}}$ expressed in the *orthonormal* Legendre basis $\{L_i\}$, the projected gradient is

$$\overline{\nabla}H(\mathbf{x}_0,\dot{\mathbf{x}}) = \mathbf{W}\otimes\left(\begin{bmatrix}\mathbf{x}_0\\ 0\end{bmatrix} + h\begin{bmatrix}1/2 & -\sqrt{3}/6\\ \sqrt{3}/6 & 0\end{bmatrix}\dot{\mathbf{x}}\right).$$

For $\dot{\boldsymbol{x}}(\tau) \in \mathbb{P}^0$ it reduces to the midpoint integration rule

$$\overline{\nabla}H(\mathbf{x}_0,\dot{\mathbf{x}}) = \mathbf{W}\left(\mathbf{x}_0 + \frac{h}{2}\dot{\mathbf{x}}\right).$$

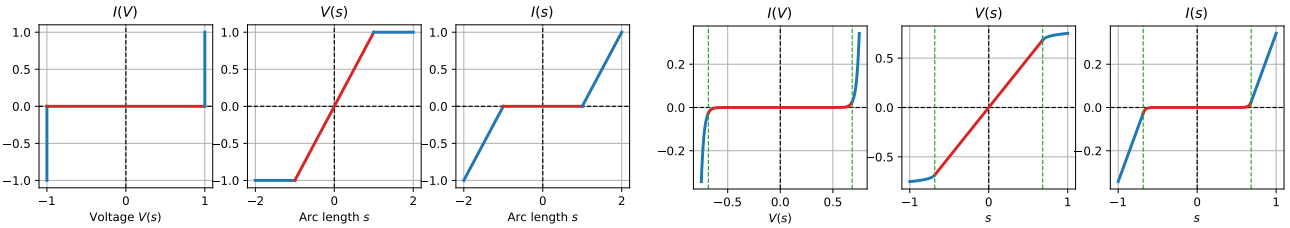

Figure 4: *(Pseudo) Arc-length parametrization of hard clipping resistor and anti-parallel Shockley diodes.*

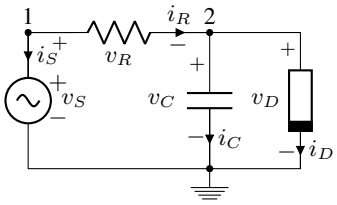

(a) Diode Clipper circuit

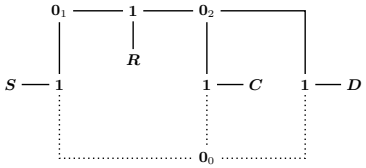

(b) Equivalent Bondgraph

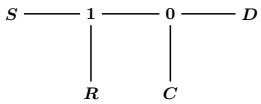

(c) Reduced Bondgraph

D	0	1	2
S	-1	1	0
R	0	1	-1
C	-1	0	1
D	-1	0	1

(d) (Reduced) Incidence Matrix

	e_1	e_2	i_S	i_R	i_C	i_D
$i_1 = 0$	.	.	-1	-1	0	0
$i_2 = 0$	.	.	0	1	-1	-1
v_S	1	0	.	.	.	.
v_R	1	-1	.	.	.	.
v_C	0	1	.	.	.	.
v_D	0	1	.	.	.	.

(e) Kirchhoff Dirac structure

	v_S	v_C	i_R	i_D
i_S	.	.	-1	0
i_C	.	.	1	-1
v_R	1	-1	.	.
v_D	0	1	.	.

(f) Reduced Hybrid Dirac structure

Figure 5: *Diode Clipper circuit: From the schematic (a) Kirchhoff laws immediately yield the bond-graph (b) which can be reduced to the bond-graph c). Using the Graph incidence matrix d), one obtains the Kirchhoff-Dirac structure e). Elimination of the node voltages yields the reduced Dirac structure f).*

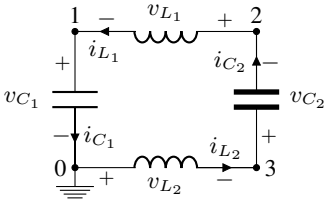

(a) LCLC circuit

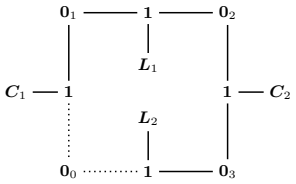

(b) Equivalent Bondgraph

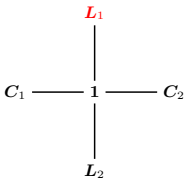

(c) Reduced Bondgraph

D	0	1	2	3
C_1	-1	1	0	0
L_1	0	-1	1	0
C_2	0	0	-1	1
L_2	1	0	0	-1

(d) (Reduced) Incidence Matrix

	e_1	e_2	e_3	i_S	i_R	i_C	i_D
$i_1 = 0$	.	.	.	-1	1	0	0
$i_2 = 0$	.	.	.	0	-1	1	0
$i_3 = 0$	.	.	.	0	0	-1	1
v_{C_1}	1	0	0	.	.	.	.
v_{L_1}	-1	1	0	.	.	.	.
v_{C_2}	0	-1	1	.	.	.	.
v_{L_2}	0	0	-1	.	.	.	.

(e) Kirchhoff Dirac structure

	v_{C_1}	v_{L_1}	v_{C_2}	i_{L_2}
i_{C_1}	.	.	.	1
i_{L_1}	.	.	.	1
i_{C_2}	.	.	.	1
v_{L_2}	-1	-1	-1	.

(f) Reduced Hybrid Dirac structure

Figure 6: *Conservative LCLC circuit (a single cell of a transmission line). There is an apparent* computational causality *conflict shown in red on subfigure f): the loop current can either be controlled by L_1 or L_2 but not by both. The circuit has thus an implicit constraint $I_{L_1}(\phi_1) = I_{L_2}(\phi_2)$. The inductor L_1 is said to have a* differential causality *since $v_{L_1} = \dot{\phi}_1$, whereas C_1, C_2, L_2 are said to have an* integral causality.